

## Perfect Stabilization of Biomolecular Adhesions under Load

Anton F. Burnet,<sup>1,2</sup> Julia Müllner,<sup>1</sup> and Benedikt Sabass<sup>1,2</sup>

<sup>1</sup>*Faculty of Physics and Center for NanoScience, Ludwig-Maximilians-Universität München, 80752 Munich, Germany*

<sup>2</sup>*Department of Veterinary Sciences, Ludwig-Maximilians-Universität München, 80752 Munich, Germany*

(Dated: March 17, 2025)

Cells attach to their environment by means of focal adhesions, which are molecular complexes that exhibit the remarkable ability to adapt to mechanical load by changing their size. Drawing from the biomolecular mechanisms underlying this behavior, we present a generic model for mechanically induced adhesion growth where conformational states of molecules already in the adhesion cluster are coupled to the adsorption of further molecules. For sufficiently strong coupling, an instability arises and unbounded system growth ensues in the absence of mechanical load. Unexpectedly, the same type of instability can lead to perfect stability under mechanical load, whereby adhesion clusters adjust their size to withstand arbitrarily large forces without breaking, a phenomenon we term perfect stabilization. We derive state diagrams that characterize adhesion stability under stationary loads and show that perfect stabilization also occurs under dynamic loading on physiologically relevant timescales. Finally, we show that perfect stabilization and related instabilities are generic phenomena that can be realized in many different ways if internal molecule states are coupled to adsorption in nonequilibrium.

A fundamental and enduring question in science is whether we can discover or engineer a material that never ruptures. Interestingly, the answer might lie in cellular adhesions, the biological glue that holds cells together. Cell-matrix adhesions, also known as focal adhesions (FA), connect the cytoskeleton to the extracellular environment and play a salient role in sensing the cell’s environment<sup>1,2</sup>, migration<sup>3</sup>, metastasis<sup>4-6</sup> and development<sup>7,8</sup>. The architecture of FAs involves transmembrane proteins called integrins that bind to the extracellular matrix (ECM) and intracellularly to adaptor proteins, notably talin, that dynamically associate and disassociate with force-generating actomyosin filaments of the cytoskeleton. This architecture has led to the characterization of FAs as molecular clutches, where the integrin-adaptor-protein unit constitute the clutch<sup>9-17</sup>.

Focal adhesions are inherently mechanosensitive; pioneering experiments have demonstrated their adaptation to local tangential forces by growing in proportion to the load<sup>18,19</sup>. Due to the system’s complexity, the underlying biological mechanisms are only partly understood. The adaptor protein talin plays a principle role in mechanosensitivity<sup>20-24</sup>. Under load, talin unfolds<sup>25</sup>, promoting integrin clustering and talin recruitment<sup>26,27</sup>, as well as adhesion reinforcement<sup>28,29</sup>. This feedback mechanism has been used to explain adaptation of FAs to ECM stiffness<sup>30</sup> and under dynamic loading<sup>31</sup>. The quest to understand the mechanosensitive growth of FAs has also prompted purely theoretical work, ranging from thermodynamic approaches<sup>32-37</sup> to stochastic modeling of the bond dynamics<sup>38-42</sup>. Basic slip-bond adhesion clusters destabilize and shrink under increasing load, see curve A in Fig. 1. However, recent work has shown that adhesion sites can grow under increasing load if the molecules they contain unfold and are exchanged with a reservoir<sup>41,42</sup>, see curve B in Fig. 1. This mechanism, termed “self-stabilization”, occurs up to a limiting force before total rupture.

This work addresses a different biophysical mechanism that affects adhesion stability. Inspired by the architecture of FAs, we consider a load-dependent adsorption rate of molecules to an existing adhesion cluster. We find that for sufficiently large coupling, the adhesion is able to withstand *arbitrarily large* static loads, see curve C in Fig. 1. This perfect stabilization results from a generic growth instability and also maintains adhesion integrity under dynamic loading of arbitrary magnitude below a certain rate threshold.

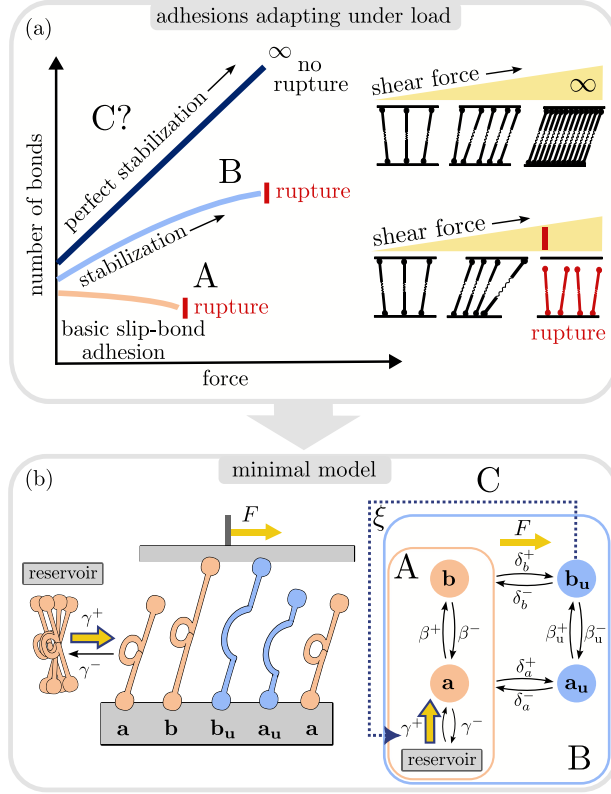


Figure 1. (a) A basic slip-bond adhesion system typically destabilizes under load, resulting in a decrease in the number of bonds (case A, orange curve). Self-stabilizing adhesion clusters exhibit an increase in bond numbers with applied force up to a critical point where bond-rupturing events dominate<sup>41</sup> (case B, light blue curve). Perfect stabilization would imply a consistent bond number increase under force, preventing rupture by keeping average molecule stretch low (case C, dark blue curve). (b) A minimal system for modeling basic slip bonds (case A), as well as self-stabilization through force-sensitive unfolding of molecules (case B). We furthermore introduce a coupling  $\xi$  (case C, dotted arrow) between force-sensitive molecule unfolding and molecule recruitment.

## I. MODEL

An adhesion is conceptualized as two parallel surfaces that are held together by a cluster of adhesion molecules, see Fig. 1(b). A shear force  $F$  acts on the upper plane and induces a displacement  $s$  and an average velocity  $v = \langle \dot{s} \rangle$ . For simplicity, all adhesion molecules are modeled as Hookean

springs with spring constant  $\kappa$  and stretch  $h$ . Furthermore, it is assumed that viscous forces are negligible so that mechanical relaxation occurs instantaneously.

We first focus on a basic slip-bond adhesion consisting only of the states  $a$  and  $b$ , highlighted as case A in Fig. 1(b). State  $a$  represents molecules that are only connected to the lower surface. Molecules coming from the surrounding bulk, termed reservoir, assemble at the adhesion site with rate  $\gamma^+$ . Dissociation of molecules from the cluster is governed by a rate coefficient  $\gamma^-$ . In state  $a$ , the molecule extension fluctuates freely with variance  $\sigma^2 = k_B T / \kappa$ , where  $k_B T$  is the thermal energy. These molecules stochastically form a bond with the upper surface, denoted by state  $b$ . The binding transition  $a \rightarrow b$  is governed by the rate coefficient  $\beta^+(h) = k_\beta \exp\left(-\frac{(h - \ell_b)^2}{2\sigma^2} + \frac{\epsilon_b}{k_B T}\right)$ , where  $k_\beta$  is the intrinsic binding rate,  $\epsilon_b$  an effective binding affinity, and  $\ell_b$  an optimal binding distance. The dissociation of a bound molecule  $b \rightarrow a$  is governed by the rate coefficient  $\beta^-(h) = k_\beta \exp\left(\frac{2|h|\ell_b - \ell_b^2}{2\sigma^2}\right)$ . The frequency of unbinding events increases with load, causing a monotonic reduction in bonds with shear force  $F$  in this basic model, until the cluster abruptly undergoes total rupture, see case A in Fig. 1(a).

The basic slip-bond model can be extended to include an unfolded molecule conformation, see case B in Fig. 1(a,b). We designate states and transition rates pertaining to unfolded molecules with a subscript  $u$ . This simple model extension can produce adhesion clusters that, as a whole, display a fundamentally different force response than individual bonds. Here, stretch shifts the state occupations to drive growth of the adhesion cluster<sup>41</sup>. Growth stabilizes adhesion clusters reversibly under force, in spite of the bond properties being the same as in the basic slip-bond model. This self-stabilization occurs up to a point of total rupture, see Fig. 1(a). Molecule unfolding is modeled as a thermally assisted jump over a single energy barrier, yielding a rate coefficient of  $\delta_{a,b}^+(h) = k_\delta \exp\left(\frac{2\Delta_1 h - \Delta_1^2}{2\sigma^2} - \frac{\epsilon_f}{k_B T}\right)$  while refolding follows  $\delta_{a,b}^-(h) = k_\delta \exp\left(\frac{-2\Delta_2 h - \Delta_2^2}{2\sigma^2}\right)$ , where  $\Delta_{1,2}$  are the distances between the metastable energy minima of the folded and unfolded states and the barrier maximum,  $\epsilon_f$  is a constant energy required for the conformation change, and  $k_\delta$  is an intrinsic rate, where we take  $k_\delta = k_\beta$ . The unfolding length is given by  $\Delta = \Delta_1 + \Delta_2$  and we assume  $\Delta_1 = \Delta_2 = \Delta/2$ . Hence, upon unfolding the stretch  $h$  relaxes to  $h - \Delta$ . All rates are defined such that the system is thermodynamically consistent at equilibrium<sup>43</sup>.

Biological FA grow in an orchestrated process where constituent molecules in different states in-

teract with each other. For example, it was recently shown that active talin molecules dimerize through interaction of their C-terminal rod domains and bind via paxillin to kindlin-2. The resulting integrin-activation complex promotes clustering of integrins<sup>50</sup>. Thus, adsorption of adhesion molecules is promoted by active molecules already in the cluster. We model this state-dependent adsorption by making the rate  $\gamma^+$  depend on the number of bound and unfolded molecules that are already in the cluster  $N_{b_u}$  as  $\gamma^+ = \gamma_0^+ + \xi N_{b_u}$ , where  $\gamma_0^+, \xi \in \mathbb{R}^+$ . See case C in Fig. 1(b). This seemingly simple modification has a profound impact on the adhesion stability, as elaborated in the following.

## II. EMERGENCE OF PERFECT STABILIZATION

We first perform stochastic simulations of the model, see Supplemental Material<sup>43</sup>. Hereafter,  $N_q$  denotes the steady-state mean number of molecules in state  $q$ . Figure 2(a) shows the number of all bound molecules  $N_B = N_b + N_{b_u}$  as a function of force  $F$  for varying coupling strength  $\xi$ . For small coupling, we observe limited self-stabilization as previously described<sup>41</sup>, where  $N_B$  initially grows with  $F$ , followed by a point of saturation and, ultimately, complete rupture. This regime of limited self-stabilization is labeled (I) in Fig. 2. Remarkably, from a critical value  $\xi \geq \xi_c$  on, the adhesion cluster size no longer saturates with increasing load and rupture is not observed in simulations. The inset in Fig. 2(a) illustrates that for  $\xi \geq \xi_c$ ,  $N_B$  versus the average bond stretch  $\bar{h}$  approaches an asymptote with increasing force, denoted  $\bar{h}_p$ . This asymptotic behavior implies together with force balance  $F = \kappa \bar{h} N_B$ , that  $N_B$  will eventually grow proportionate to  $F$  while the average stretch attains a finite constant. We refer to this regime as *perfect* stabilization, labeled (II) in Fig. 2. The critical value  $\xi_c$  corresponds to the coupling at which the rupture force in regime (I) reaches infinity. An increase of  $\xi$  beyond  $\xi_c$  results in stronger cluster growth with force, maintaining smaller average stretches, until the asymptote  $\bar{h}_p$  reaches zero for coupling  $\xi^*$ , marking the onset of an unbounded growth regime, where the system grows indefinitely. The regime of unbounded growth occurs for any force  $F \geq 0$ . Thus, the perfect stabilization emerges in the bounded interval  $\xi_c \leq \xi < \xi^*$ . The different regimes are summarized in Fig. 2(b).

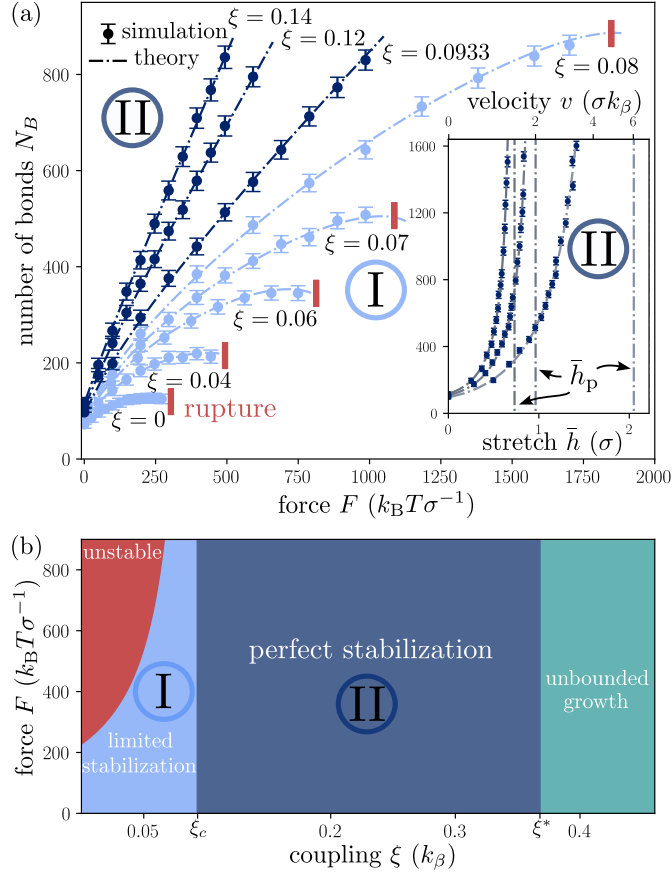


Figure 2. Simulation results for the model shown in Fig. 1(b). Dashed lines show mean-field solutions. (a) For small coupling  $\xi$ , the mean number of bound molecules in steady state  $N_B$  initially grows with force up to a point of saturation (light blue). Red bars indicate a complete rupture of adhesion clusters in simulations. With  $\xi$  increasing, the rupture forces increase. For  $\xi \geq \xi_c \approx 0.0933 k_\beta$ , adhesions no longer rupture in the simulations (dark blue). Inset of (a):  $N_B$  plotted against  $\bar{h}$  and  $v$  for  $\xi \in \{0.0933, 0.12, 0.14\} k_\beta$ .  $N_B$  diverges for large loads at finite average stretches  $\bar{h} = \bar{h}_p$ . (b) State diagram for adhesion stability. For  $0 \leq \xi < \xi_c$ , the adhesions self-stabilize in a finite range of forces. For  $\xi_c \leq \xi < \xi^*$ , the model stabilizes perfectly. For  $\xi \geq \xi^*$ , the system grows indefinitely.

### III. MEAN-FIELD APPROXIMATION

To understand the critical behavior of the adhesion system illustrated in Fig. 2, it is sufficient to consider an approximate model in which we decouple the stretch variables of individual bonds from each other by assuming, instead of a constant force  $F$ , a constant velocity  $v$ . We describe an ensemble of molecules by functions  $n_q(h)$ , representing the number of molecules in a state  $q$  with stretch  $h$ . The governing equations for  $q, p \in \{a, a_u, b, b_u\}$  at steady state read

$$\begin{aligned} \partial_t n_q(h) = 0 = & \sum_p [k^{p \rightarrow q}(h)n_p(h) - k^{q \rightarrow p}(h)n_q(h)] \\ & - (\delta_{q,b} + \delta_{q,b_u})v \partial_h n_q(h) + \delta_{q,a} \eta(h)(\gamma_0^+ + \xi N_{b_u}), \end{aligned} \quad (1)$$

where  $k^{p \rightarrow q}$  denotes the transition rates from state  $p$  to state  $q$  in the scheme shown in Fig. 1(b) and  $\eta(h)$  denotes the normalized Gaussian distribution  $\eta(h) \sim \mathcal{N}(0, \sigma^2)$ , where for  $q \in \{a, a_u\}$ ,  $n_q(h) = N_q \eta(h)$ . Note that the unfolded molecule states have a shifted stretch coordinate  $h - \Delta$ . For the bound molecules  $q \in \{b, b_u\}$ , the right-hand side of Eq. (1) is supplemented with the expression  $-v \partial_h n_q(h)$  to account for bond stretch due to the relative motion of the planes. Accordingly, the average stretch  $\bar{h} = \bar{h}(v)$  and, due to linearity, is independent of  $\xi$ <sup>43</sup>. For the following, we introduce convenient stretch-averaged effective rates as

$$\bar{k}^{p \rightarrow q} = \int_{\mathbb{R}} dh \frac{n_p(h)}{N_p} k^{p \rightarrow q}(h). \quad (2)$$

#### A. Instability of equilibrium solution above $\xi^*$

The approximate model becomes exact at equilibrium, where  $F = 0$ ,  $v = 0$ , and  $\bar{h} = 0$ . Since molecule extensions obey here Gaussian distributions, the effective rates are easily calculated. The equilibrium number of molecules in state  $q$  is  $N_q^*(\xi) \propto 1/(\gamma^- k^{\rightarrow a} - \xi k^{\rightarrow b_u})$ , where  $k^{\rightarrow q} \equiv \sum_{\mu} \prod_{(p', q') \in \mathcal{T}_{\mu}^q} \bar{k}^{p' \rightarrow q'}$ , which denotes the sum of products of rates  $\bar{k}^{p' \rightarrow q'}$  associated with the edge  $(p', q')$  that belongs to the  $\mu$ -th spanning tree of the network graph, shown in Fig. 1(b), with edges directed towards  $q$ ,  $\mathcal{T}_{\mu}^q$ . At  $\xi^* \equiv \gamma^- \frac{k^{\rightarrow a}}{k^{\rightarrow b_u}} = \gamma^- e^{-(\epsilon_b - \epsilon_f)/k_B T}$ <sup>51</sup>, the system size diverges as a result of a flux imbalance at the reservoir.

## B. Perfect stabilization under load above $\xi_c$

Under load, the bond stretch distributions deviate from a Gaussian and shift in the direction of the applied force, resulting in a non-zero average stretch  $\bar{h}$ , as depicted in Fig. 3(a). Due to linearity, the normalized stretch distributions  $n_{b(u)}/N_{b(u)}$ , which can be solved numerically from the mean-field equations (1) for a given  $\bar{h}$ , are independent of  $\xi$ <sup>43</sup>. Consequently, the four  $\bar{h}$ -dependent effective rates  $\bar{\beta}^-(\bar{h}), \bar{\beta}_u^-(\bar{h}), \bar{\delta}_b^+(\bar{h})$  and  $\bar{\delta}_b^-(\bar{h})$  are also independent of  $\xi$ . These effective rates encapsulate the information of the shifting distributions governed by Eq. (1), see Fig. 3(b). The mean number of bound molecules is therewith given by

$$N_B(\bar{h}, \xi) = \frac{\gamma_0^+ [k^{\rightarrow b}(\bar{h}) + k^{\rightarrow b_u}(\bar{h})]}{\gamma^- k^{\rightarrow a}(\bar{h}) - \xi k^{\rightarrow b_u}(\bar{h})}. \quad (3)$$

Solutions of Eq. (3) are in excellent agreement with simulation results, as shown in Fig. 2(a).

To see how Eq. (3) explains perfect stabilization in the range  $\xi_c \leq \xi < \xi^*$ , consider regime (II) in the state diagram shown in Fig. 3(c), corresponding to (II) in Fig. 2(b). The line denoted by  $\bar{h}_p(\xi)$ , where  $\xi k^{\rightarrow b_u}(\bar{h}_p(\xi)) = \gamma^- k^{\rightarrow a}(\bar{h}_p(\xi))$ , forms a boundary between regime (II) and unbounded growth. This boundary marks the onset of positivity in the largest eigenvalue of the system described by the effective rates, which we hereafter refer to as the effective eigenvalue. The end points of the critical line,  $\xi_c$  and  $\xi^*$ , are located at  $\bar{h} = \sup \bar{h}_R$  and  $\bar{h} = 0$ , respectively, where  $\bar{h}_R \in \{\bar{h} \mid N_B(\bar{h}, \xi) = \max_{\bar{h}'} N_B(\bar{h}', \xi)\}$  denotes the destabilization boundary in regime (I). Assume that the system state is initially in (II) close to the critical line. If the load per bond increases, either through fluctuations or through external influence,  $\bar{h}$  will grow. However, the system cannot attain a steady state with an average stretch exceeding  $\bar{h}_p$ , as the onset of unbounded growth at this point reduces the average stretch below  $\bar{h}_p$ . This effect bounds the growth of  $\bar{h}$ , thereby preventing rupture. Thus, while the divergent growth under load for  $\xi_c \leq \xi < \xi^*$  mirrors the equilibrium instability, it enables perfect stability of the adhesion cluster.

## C. Broad range of perfect stabilization

The condition for perfect stabilization can be visualized graphically by crossings of the numerically calculated functions  $k^{\rightarrow b_u}$  and  $k^{\rightarrow a}$ , which yields  $\bar{h}_p$ ; see inset of Fig. 3 (c).



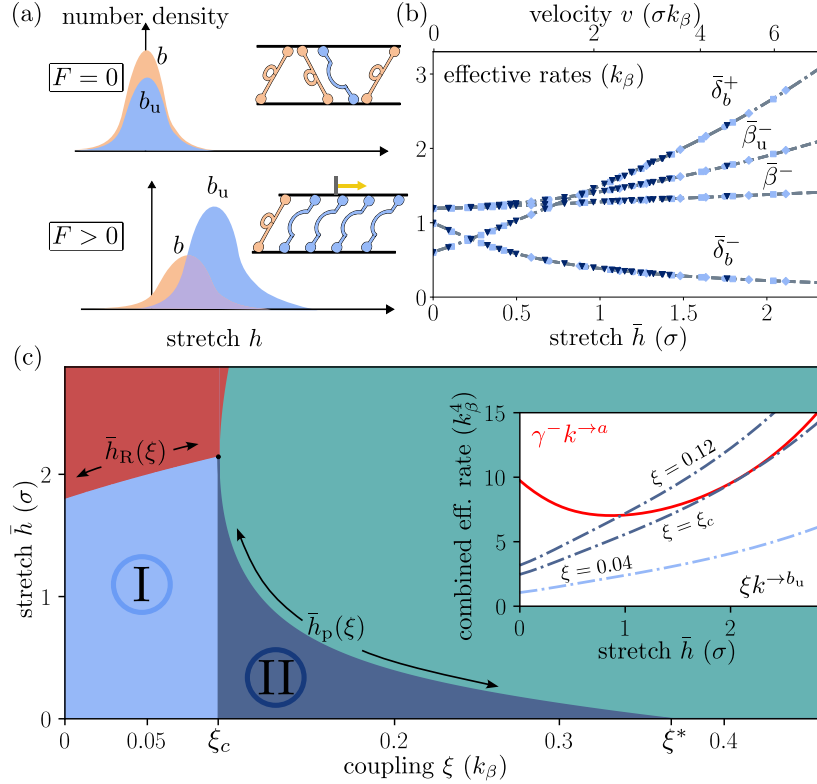


Figure 3. (a) Illustration of the molecule stretch distributions in and out of equilibrium. Forces on the adhesion clusters stretch the bonds, which in turn promotes unfolding of the molecules. (b) Effective transition rates as a function of average stretch  $\bar{h}$ . Dashed lines are numerical results from the mean-field equations, symbols are results from stochastic simulations (for various  $\xi$ , both non-critical and critical.) (c) State diagram for adhesion stability as a function of average stretch  $\bar{h}$ , corresponding to Fig. 2(b). Perfect stabilization occurs in region (II), where  $\xi_c \leq \xi < \xi^*$  and  $\bar{h} < \bar{h}_p(\xi)$ . The cluster grows without bounds on the line  $\bar{h} = \bar{h}_p(\xi)$ . The inset illustrates the competition between  $\gamma^- k^{\rightarrow a}$  and  $\xi k^{\rightarrow b_u}$  (defined in the main text) with increasing  $\bar{h}$  for varying  $\xi$ . The points at which the curves cross determine average stretch values  $\bar{h}_p$  for onset of divergent growth as  $\gamma^- k^{\rightarrow a} = \xi k^{\rightarrow b_u}$ .

A broad range  $[\xi_c, \xi^*)$  is characterized by strong growth of  $k^{\rightarrow b_u}$  with respect to  $k^{\rightarrow a}$ . This range depends on the system parameters but is typically broad for physiologically relevant scales, see Supplemental Material<sup>43</sup>. Particularly important are the parameters controlling the accessibility (e.g.,  $\epsilon_f$  and  $\epsilon_b$ ) and the mechanosensitivity ( $\Delta$  and  $\ell_b$ ) of the bound molecules. For the limit of

force insensitive folding transitions  $\Delta \rightarrow 0$ , we find  $\xi_c \rightarrow \xi^*$ , highlighting the crucial feature of force-sensitive coupling.

#### IV. DYNAMIC LOADING

To go beyond the static load assumption made so far, we next study linear force ramps. In the simulations, force ramps are approximated by incrementally increasing the force by an amount  $dF$  at fixed time intervals  $dt$ , so that an effective loading rate is given by  $\dot{F} = dF/dt$ <sup>43</sup>. For intrinsic binding rates relevant in cell adhesions  $k_\beta \sim 10^{-1} - 10^1 \text{ s}^{-1}$ <sup>52</sup>, loading rates  $\sim 10^0 - 10^2 k_B T \sigma^{-1} k_\beta \sim 10^{-1} - 10^3 \text{ pNs}^{-1}$  are consistent with physiologically relevant scales<sup>53,54</sup>. For regimes (I) and (II), we find a limiting loading rate  $\dot{F}_{\text{ss}}$ , below which the system's transient response closely approximates the steady-state limit independently of  $\xi$ , where, numerically,  $\dot{F}_{\text{ss}} \approx 1.7 k_B T \sigma^{-1} k_\beta$ <sup>55</sup>. For  $\dot{F} > \dot{F}_{\text{ss}}$ , in regime (II), the system can overshoot beyond  $\bar{h}_p$ , developing a positive effective eigenvalue before either stabilizing or rupturing. During a stable overshoot, the average stretch decreases due to cluster growth and eventually reaches a value close to the asymptote  $\bar{h}_p$ , where perfect stabilization is achieved, see sample trajectory in Fig. 4(a). The effective eigenvalue peaks at a positive value at average stretches of  $\bar{h}^{\lambda_{\text{max}}}$  before returning to negative values at  $\bar{h}_{p,2}$ , see Fig. 4(b). Thus, the domain  $[\bar{h}_p, \bar{h}_{p,2}]$  acts as a stabilizing stretch buffer against perturbations and fluctuations<sup>43</sup>. Stable overshoots occur if loading rates are smaller than  $\dot{F}_{\text{lim}} \approx \kappa N_B^i (\bar{h}^{\lambda_{\text{max}}} - \bar{h}^i) / \tau_{\text{resp}}$ , where  $\tau_{\text{resp}}$  characterizes a lag time resulting from the growth dynamics and  $N_B^i$  and  $\bar{h}^i$  are the steady-state quantities before commencement of loading. Note that the value for  $\dot{F}_{\text{lim}}$  is dependent on the initial state of the cluster. For loading proximate to the asymptote, as  $\xi \rightarrow \xi_c$ ,  $\bar{h}_{p,2} - \bar{h}_p \rightarrow 0$  and so  $\dot{F}_{\text{lim}} \rightarrow \dot{F}_{\text{ss}}$ .

Figure 4(c) shows sample trajectories for which the force ramp starts from a steady state close to  $\bar{h}_p$  with  $\xi = 0.12 k_\beta > \xi_c$ . For  $\dot{F} > \dot{F}_{\text{lim}}$ , after the lag time  $\sim \tau_{\text{resp}}$ , the positive effective eigenvalue decreases with increasing stretch, reducing the growth response despite rising forces. Consequently, the cluster average stretch can diverge. Note the broad range of loading rates that allow stabilization beyond the limit of quasi-static perfect stabilization  $\dot{F}_{\text{lim}} \gg \dot{F}_{\text{ss}}$ , see inset Fig. 4(c) and Supplemental Material<sup>43</sup>.

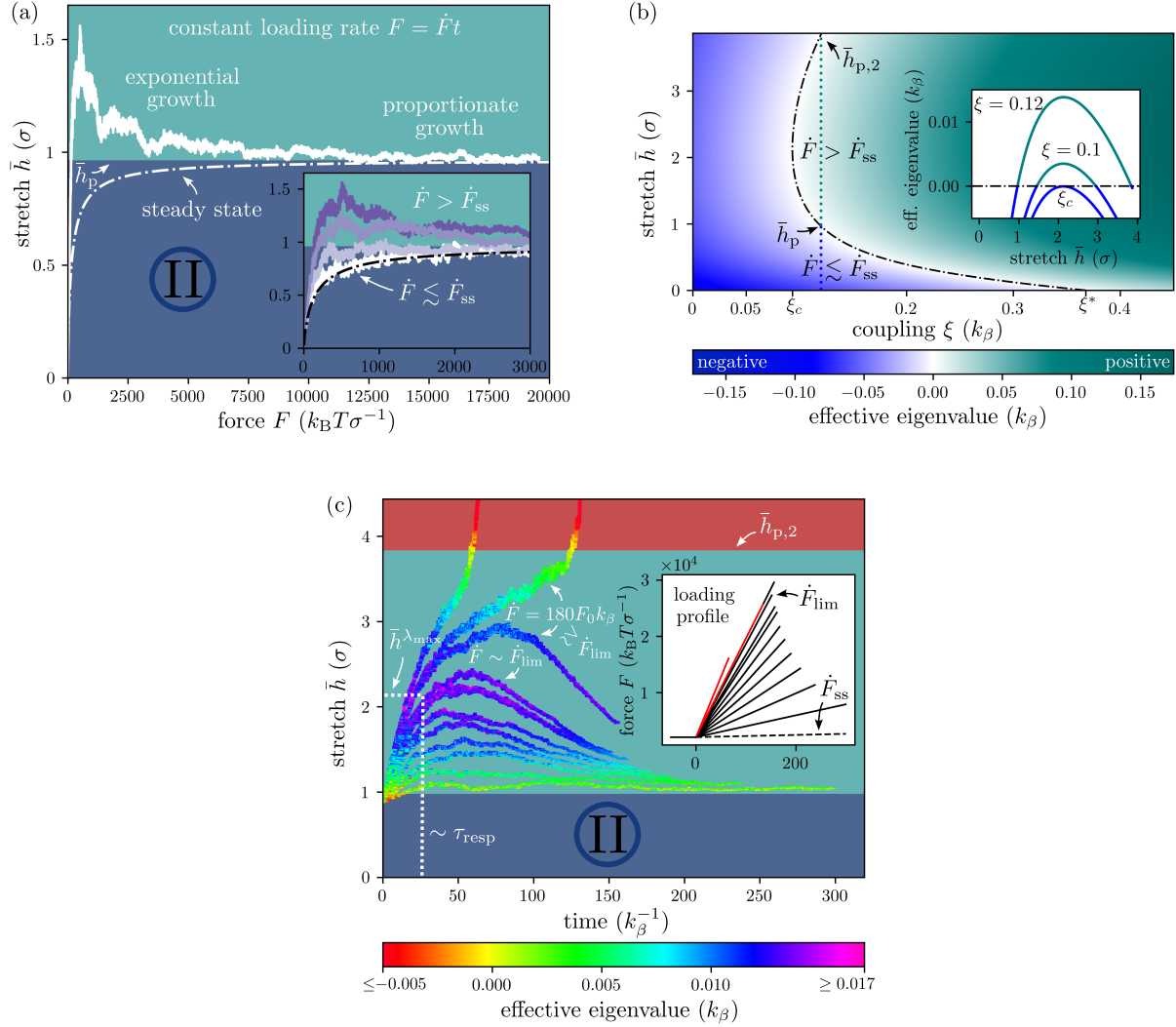


Figure 4. Dynamic loading. (a) A sample trajectory for  $\xi = 0.12 k_\beta$ , with constant loading rate  $\dot{F} = 15 F_0 k_\beta$  ( $F_0 = k_B T \sigma^{-1}$ ) starting from  $F = 0$ . The system passes beyond  $\bar{h}_p$ , undergoes exponential growth followed by proportional growth with force. Inset: sample trajectories with  $\dot{F} \in \{1, 5, 11, 15\} F_0 k_\beta$ . (b) Largest effective eigenvalue distribution estimated from the mean-field solutions. For  $\dot{F} > \dot{F}_{ss}$ , the system can develop a positive effective eigenvalue. Inset shows cuts for three values of the control parameter  $\xi$ . (c) Sample trajectories with  $\dot{F} \in \{20, 40, \dots, 120, 140, 150, 170, 180, 220\} F_0 k_\beta$  showing transient exponential growth and instabilities for force ramps starting at a steady state near  $\bar{h}_p$  with  $\xi = 0.12 k_\beta$ . Effective eigenvalue is computed from simulations. Inset: loading profiles for each plotted trajectory. For  $\dot{F} > \dot{F}_{lim} \approx 170 F_0 k_\beta$ , the system can become unstable (red lines).

## V. PERFECT STABILIZATION IN GENERIC NETWORKS

In the aforementioned model, the unfolded states act as force sensors. However, we also find perfect stabilization can arise in an even simpler two-state model, where adsorption depends on the bound-state stretches that serve to detect force, see Supplemental Material<sup>43</sup>. Therefore, we consider a generic connected network representing bound and unbound states with an arbitrary number of reservoir connections coupled to an arbitrary number of internal states. It can be shown that the stationary nonequilibrium occupation number of a state  $q$  obeys

$$N_q(\bar{h}, \xi) \propto \frac{1}{\sum_{i \in \mathcal{I}} \nu_i k^{\rightarrow a_i}(\bar{h}) - \xi \sum_{j \in \mathcal{J}} k^{\rightarrow p_j}(\bar{h})}, \quad (4)$$

where  $\mathcal{I}$  and  $\mathcal{J}$  index the reservoir connections and coupled states, respectively, and  $\nu_i$  ensure Kolmogorov cycle criterion is satisfied. In direct analogy with the special case studied above, any  $k^{\rightarrow p_j}(\bar{h})$  that increase with load can drive load-dependent adsorption of molecules and lead to perfect stabilization in a broad class of networks representing complex biomolecular adhesion clusters.

## VI. CONCLUDING PERSPECTIVE

Using a minimal model in which the recruitment of molecules to an adhesion cluster is determined by the internal states of the molecules already in the cluster, we show how biomolecular adhesion can achieve perfect stability by adjusting its size to any load. This perfect stabilization is distinct from the mechanism of limited self-stabilization<sup>41,42</sup>, which leads to regime (I) in Fig. 2. Albeit similarly reliant on molecule recruitment and force-sensitive transitions, perfect stabilization can occur in models that, without coupling, are unable to self-stabilize<sup>43</sup>. While biochemical reactions are often diffusion-limited, our assumed force-dependent molecule adsorption rate is consistent with the force-induced exposure of cryptic binding sites and phosphorylation-controlled activation of adaptor proteins in focal adhesions<sup>56,57</sup>, which are thought to have a large influence on affinities.

Although inspired by focal adhesions, this versatile model can be extended in future to incorporate details of various other types of cell adhesions and help to unravel the principles governing these complex nanomechanical structures. Furthermore, it would be interesting to explicitly model the

load-dependent molecule adsorption through multimolecular interactions, which naturally give rise to nonequilibrium growth instability<sup>58,59</sup>. From a material science perspective, our model also offers an initial blueprint for the development of non-rupturing junctions, with potential applications in material design and engineering.

## ACKNOWLEDGEMENTS

We acknowledge funding by the European Research Council (ERC) under the European Union’s Horizon 2020 research and innovation programme (BacForce, G.A.No. 852585) and by the Deutsche Forschungsgemeinschaft (DFG, German Research Foundation), Project no 492014049.

## REFERENCES

- <sup>1</sup>B. Geiger, J. P. Spatz, and A. D. Bershadsky, *Nat. Rev. Mol. Cell Bio.* **10**, 21 (2009).
- <sup>2</sup>I. Schoen, B. L. Pruitt, and V. Vogel, *Annu. Rev. Mater. Res.* **43**, 589 (2013).
- <sup>3</sup>A. Huttenlocher and A. R. Horwitz, *C.S.H Perspect. Biol.* **3**, a005074 (2011).
- <sup>4</sup>D. T. Butcher, T. Alliston, and V. M. Weaver, *Nat. Rev. Cancer* **9**, 108 (2009).
- <sup>5</sup>S. C. Schwager, P. V. Taufalele, and C. A. Reinhart-King, *Cell. Mol. Bioeng.* **12**, 1 (2019).
- <sup>6</sup>Y. Xin, K. Li, M. Huang, C. Liang, D. Siemann, L. Wu, Y. Tan, and X. Tang, *Oncogene* **42**, 3457 (2023).
- <sup>7</sup>A. J. Engler, S. Sen, H. L. Sweeney, and D. E. Discher, *Cell* **126**, 677 (2006).
- <sup>8</sup>C.-P. Heisenberg and Y. Bellaïche, *Cell* **153**, 948 (2013).
- <sup>9</sup>T. Mitchison and M. Kirschner, *Neuron* **1**, 761 (1988).
- <sup>10</sup>M. L. Gardel, B. Sabass, L. Ji, G. Danuser, U. S. Schwarz, and C. M. Waterman, *J. Cell Biol.* **183**, 999 (2008).
- <sup>11</sup>B. Sabass and U. S. Schwarz, *J. Phys. Condens. Mat.* **22**, 194112 (2010).
- <sup>12</sup>Y. Li, P. Bhimalapuram, and A. R. Dinner, *J. Phys. Condens. Mat.* **22**, 194113 (2010).
- <sup>13</sup>S. W. Moore, P. Roca-Cusachs, and M. P. Sheetz, *Dev. Cell* **19**, 194 (2010).
- <sup>14</sup>P. Sens, *Europhys. Lett.* **104**, 38003 (2013).

- <sup>15</sup>Z. Sun, S. S. Guo, and R. Fässler, *J. Cell Biol.* **215**, 445 (2016).
- <sup>16</sup>C. E. Chan and D. J. Odde, *Science* **322**, 1687 (2008).
- <sup>17</sup>A. Elosegui-Artola, X. Trepas, and P. Roca-Cusachs, *Trends Cell Biol.* **28**, 356 (2018).
- <sup>18</sup>D. Riveline, E. Zamir, N. Q. Balaban, U. S. Schwarz, T. Ishizaki, S. Narumiya, Z. Kam, B. Geiger, and A. D. Bershadsky, *J. Cell Biol.* **153**, 1175 (2001).
- <sup>19</sup>N. Q. Balaban, U. S. Schwarz, D. Riveline, P. Goichberg, G. Tzur, I. Sabanay, D. Mahalu, S. Safran, A. Bershadsky, L. Addadi, *et al.*, *Nat. Cell Biol.* **3**, 466 (2001).
- <sup>20</sup>S. E. Lee, R. D. Kamm, and M. R. Mofrad, *J. Biomech.* **40**, 2096 (2007).
- <sup>21</sup>J. Yan, M. Yao, B. T. Goult, and M. P. Sheetz, *Cell. Mol. Bioeng.* **8**, 151 (2015).
- <sup>22</sup>A. Kumar, M. Ouyang, K. Van den Dries, E. J. McGhee, K. Tanaka, M. D. Anderson, A. Groisman, B. T. Goult, K. I. Anderson, and M. A. Schwartz, *J. Cell Biol* **213**, 371 (2016).
- <sup>23</sup>B. Klapholz and N. H. Brown, *J. Cell Sci.* **130**, 2435 (2017).
- <sup>24</sup>B. T. Goult, J. Yan, and M. A. Schwartz, *J. Cell Biol.* **217**, 3776 (2018).
- <sup>25</sup>A. Del Rio, R. Perez-Jimenez, R. Liu, P. Roca-Cusachs, J. M. Fernandez, and M. P. Sheetz, *Science* **323**, 638 (2009).
- <sup>26</sup>C. Cluzel, F. Saltel, J. Lussi, F. Paulhe, B. A. Imhof, and B. Wehrle-Haller, *J. Cell Biol.* **171**, 383 (2005).
- <sup>27</sup>P. Roca-Cusachs, N. C. Gauthier, A. Del Rio, and M. P. Sheetz, *Proc. Natl. Acad. Sci. U.S.A* **106**, 16245 (2009).
- <sup>28</sup>M. Yao, B. T. Goult, H. Chen, P. Cong, M. P. Sheetz, and J. Yan, *Sci. Rep. U.K.* **4**, 4610 (2014).
- <sup>29</sup>M. Yao, B. T. Goult, B. Klapholz, X. Hu, C. P. Toseland, Y. Guo, P. Cong, M. P. Sheetz, and J. Yan, *Nat. Commun.* **7**, 11966 (2016).
- <sup>30</sup>A. Elosegui-Artola, R. Oria, Y. Chen, A. Kosmalska, C. Pérez-González, N. Castro, C. Zhu, X. Trepas, and P. Roca-Cusachs, *Nat. Cell Biol.* **18**, 540 (2016).
- <sup>31</sup>I. Andreu, B. Falcones, S. Hurst, N. Chahare, X. Quiroga, A.-L. Le Roux, Z. Kechagia, A. E. Beedle, A. Elosegui-Artola, X. Trepas, R. Farre, T. Betz, I. Almendros, and P. Roca-Cusachs, *Nat. Commun.* **12**, 4229 (2021).
- <sup>32</sup>A. Nicolas, B. Geiger, and S. A. Safran, *Proc. Natl. Acad. Sci. U.S.A* **101**, 12520 (2004).

- <sup>33</sup>T. Shemesh, B. Geiger, A. D. Bershadsky, and M. M. Kozlov, Proc. Natl. Acad. Sci. U.S.A **102**, 12383 (2005).
- <sup>34</sup>A. Besser and S. A. Safran, Biophys. J. **90**, 3469 (2006).
- <sup>35</sup>A. Nicolas, A. Besser, and S. A. Safran, Biophys. J. **95**, 527 (2008).
- <sup>36</sup>A.-S. Smith, K. Sengupta, S. Goennenwein, U. Seifert, and E. Sackmann, Proc. Natl. Acad. Sci. U.S.A. **105**, 6906 (2008).
- <sup>37</sup>J. E. Olberding, M. D. Thouless, E. M. Arruda, and K. Garikipati, PLoS One **5**, e12043 (2010).
- <sup>38</sup>D. Kong, B. Ji, and L. Dai, J. Biomech. **43**, 2524 (2010).
- <sup>39</sup>H. Gao, J. Qian, and B. Chen, J. R. Soc. Interface **8**, 1217 (2011).
- <sup>40</sup>R. De, Commun. Biol. **1**, 81 (2018).
- <sup>41</sup>A. Braeutigam, A. N. Simsek, G. Gompper, and B. Sabass, Nat. Commun. **13**, 2197 (2022).
- <sup>42</sup>A. Braeutigam, A. F. Burnet, G. Gompper, and B. Sabass, J. Phys. Condens. Mat. (2024).
- <sup>43</sup>See Supplemental Material for further model and simulation details, mean-field results and derivations, and model variations, which includes the Refs.<sup>44–49</sup>.
- <sup>44</sup>M. Dembo, D. Torney, K. Saxman, and D. Hammer, Proc. R. Soc. B. Biol. Sci. **234**, 55 (1988).
- <sup>45</sup>T. L. Hill, J. Theor. Biol. **10**, 442 (1966).
- <sup>46</sup>J. Schnakenberg, Rev. Mod. Phys. **48**, 571 (1976).
- <sup>47</sup>W. Magnus, Commun. Pure Appl. Math. **7**, 649 (1954).
- <sup>48</sup>D. T. Gillespie, J. Comput. Phys. **22**, 403 (1976).
- <sup>49</sup>D. T. Gillespie, J. Phys. Chem. **81**, 2340 (1977).
- <sup>50</sup>F. Lu, L. Zhu, T. Bromberger, J. Yang, Q. Yang, J. Liu, E. F. Plow, M. Moser, and J. Qin, Nat. Commun. **13**, 2362 (2022).
- <sup>51</sup>The steady-state probability  $p_q \propto k^{\rightarrow q}$ <sup>43</sup>. Accordingly, the term  $\gamma^- \frac{k^{\rightarrow a}}{k^{\rightarrow b_u}} = \gamma^- \frac{p_a}{p_{b_u}}$ . Indeed, by local detailed balance, at equilibrium the steady-state probability ratio follows a Boltzmann distribution  $\frac{p_a}{p_{b_u}} = e^{-(\epsilon_b - \epsilon_f)/k_B T}$  where  $\epsilon_b - \epsilon_f$  corresponds to the free energy difference between the  $a$  and  $b_u$  states.
- <sup>52</sup>T. Bihl, S. Fenz, E. Sackmann, R. Merkel, U. Seifert, K. Sengupta, and A.-S. Smith, Biophys. J. **107**, L33 (2014).
- <sup>53</sup>E. A. Evans and D. A. Calderwood, Science **316**, 1148 (2007).

- <sup>54</sup>M. H. Jo, P. Meneses, O. Yang, C. C. Carcamo, S. Pangeni, and T. Ha, *Science* **383**, 1374 (2024).
- <sup>55</sup>To estimate  $\dot{F}_{ss}$ , we apply a force step  $\delta F$  to a steady state and measure the time  $\delta t$  to the next steady state, such that  $\dot{F}_{ss} \approx \delta F / \delta t$ . See Supplemental Material<sup>43</sup>.
- <sup>56</sup>K. Austen, P. Ringer, A. Mehlich, A. Chrostek-Grashoff, C. Kluger, C. Klingner, B. Sabass, R. Zent, M. Rief, and C. Grashoff, *Nat. Cell Biol.* **17**, 1597 (2015).
- <sup>57</sup>J. Zhou, C. Aponte-Santamaría, S. Sturm, J. T. Bullerjahn, A. Bronowska, and F. Gräter, *PLoS Comput. Biol.* **11**, e1004593 (2015).
- <sup>58</sup>S. G. Marehalli Srinivas, F. Avanzini, and M. Esposito, *Phys. Rev. Lett.* **132**, 268001 (2024).
- <sup>59</sup>S. G. Marehalli Srinivas, F. Avanzini, and M. Esposito, *Phys. Rev. E* **109**, 064153 (2024).